engineering. Journal of Engineering Design, 20(6) p.p.589-607.
9. Liu, S., Lin, Y., Forrest, J. Y. L. (2010) Grey systems: theory and applications. Springer Science & Business Media: Berlin.
10. Long, H., Wang, L., Shen, J., Wu, M., Jiang, Z. (2013) Product service system configuration based on support vector machine considering customer perception. International Journal of Production Research, 51(18) p.p.5450-5468.
11. Nagamachi, M. 1995. Kansei Engineering: A new ergonomic consumer-oriented technology for product development. International Journal of Industrial Ergonomics, 15(94) p.p. 3–11.
12. Nishino, T., Nagamachi, M., Tanaka, H. (2006) Variable precision Bayesian rough set model and its application to Kansei engineering, Transactions on Rough Sets V, p.p.190-206.
13. Schütte*, S. T., Eklund, J., Axelsson, J. R., Nagamachi, M. (2004) Concepts, methods and tools in Kansei Engineering. Theoretical Issues in Ergonomics Science, 5(3) p.p. 214-231.
14. Shi, F., Sun, S., Xu, J. (2012) Employing rough sets and association rule mining in KANSEI knowledge extraction. Information Sciences, 196 p.p.118-128.
15. Smith, S., & Fu, S.-H. (2011) The relationships between automobile head-up display presentation images and drivers' Kansei. Displays, 32(2) p.p. 58-68.
16. Su, J., Li, H (2005) Investigation of relationship of form design elements to kansei image by means of quantification-I theory. Journal of lanzhou University of Technology, 31(2) p.p. 36-39.
17. Yang, C.C. (2011) A classification-based Kansei engineering system for modeling consumers' affective responses and analyzing product form features. Expert Systems with Applications, 38(9) p.p.11382-11393.
18. Zhai, L.-Y., Khoo, L.-P., Zhong, Z.W. (2009) A dominance-based rough set approach to Kansei Engineering in product development. Expert Systems with Applications, 36(1) p.p. 393-402.
19. Zhang, Y., Yang, J., Jiang, H. (2012) Machine tool thermal error modeling and prediction by grey neural network. The International Journal of Advanced Manufacturing Technology, 59(9-12) p.p. 1065-1072.

Optimization and Experiment on the Main Direction of Incremental Forming

Guangcheng Zha[1,2], Xiaofan Shi[1,2], Wei Zhao[1,2], Fanxin Kong[1,2], Chuankai Lu[1], Menglin Wu[1,2]

[1] School of Materials Science and Engineering, Nanjing Institute of Technology, Nanjing 211167, Jiangsu, China
[2] Jiangsu Key Laboratory of Advanced Structural Materials and Application Technology, Nanjing 211167, Jiangsu, China

Abstract
In the incremental forming process, the change in material thickness is related to the spatial placement direction of a workpiece (the main direction of incremental forming), which is the key to ensure the reasonable thickness of parts. The forming parts model is divided into stereolithography (STL) triangle meshes with reasonable accuracy. The angle between the normal vector and the z-axis is considered the forming angle θ of the position. According to the law of cosines of the thickness of incremental forming $t = t_0 * \cos\theta$, the rotation matrix of the normal vector is obtained on the basis of the constrained condition of part thickness. As such, the overall rotation of the STL model is achieved, and the spatial forming position of the workpiece model is determined. In this study, typical free-curved surface parts are selected. Experimental results show that the method can determine the ideal thickness of a workpiece. Hence, this work can serve as a reference when determining the reasonable thickness distribution of complex parts according to random and optimized placement.
Key words: INCREMENTAL FORMING, MAIN FORMING DIRECTION, STL FILE, THICKNESS ANALYSIS.

1. Introduction

Incremental sheet forming is a flexible dieless forming technology used to discretize a three-dimensional model into a series of two-dimensional contour models and obtain the overall shape of parts through local plastic forming accumulation[1–3]. This forming technology was proposed by the American scholar Leszak[4] in the 1960s.

In the 1990s, this technology gradually attracted the attention of scholars in various countries because of the related work conducted by Matsuhara Shio (Japan) and others[5-6]. Today, incremental forming is one of the advanced processing technologies for metal sheet plastic forming because of its low forming force, energy consumption, vibration, and noise[7–10]. Numerous scholars in China and abroad have conducted research on the field of incremental forming technology, incremental forming mechanism, and numerical simulations.

Hirt[11] and others proposed that the change in material thickness in incremental forming follows the law of cosines $t = t_0 * \cos\theta$ (the forming angle θ is the angle between the normal vector of the processing position and the *z*-axis). The overall direction of the position of incremental forming parts (hereinafter referred to as the main direction of incremental forming) will affact the forming angle θ and thickness value of different position of parts.

In the present study, a new method based on the stereolithography (STL) file format for determining the main direction of incremental forming is proposed to provide a reference for incremental forming. For structural parts, the main direction of incremental forming affects mechanical properties and the subsequent assembly of parts that are thin or have varied thicknesses[12]. In practice, the main direction of incremental forming parts is manually positioned on the basis of experience; hence, this approach cannot achieve ideal processing effects. The STL file format is a three-dimensional graphics file format for rapid prototyping and manufacturing technology services. This file format represents an object contour model as a collection of triangle meshes. The STL file format has been extensively used in animation, virtual reality, and rapid prototyping.

2. Optimization of the main forming direction

2.1 Optimization theory of the main forming direction

The optimization of the main forming direction ensures that the model of parts generates a precise STL file and that the surface of the model is discretized into triangle meshes. When the precision is reasonable, the normal vector of optional position on the curved surface could be replaced by the outer normal vector of the triangle mesh. The angle between the vector and the *z*-axis can be considered as the incremental forming angle θ of this position. The optimization of the main forming direction substantially controls the normal vector of the STL triangle mesh, causing it to revolve according to a certain condition. Moreover, this optimization leads to a reasonable angle, that is, the forming angle θ between the normal vector of the triangle meshes and the *z*-axis. Then, the vertex coordinates of each triangle mesh are calculated after revolving according to the rotation matrix when the normal vector is rotated in place. The spatial STL model obtained through the aforementioned process indicates the processing position of the parts. The incremental forming process code can then be generated directly on the basis of this model.

2.2 Information and expression of the STL file

As shown in Figure 1, the information unit of STL triangle meshes includes the coordinate value of three vertices, namely, v_{ix}, v_{iy}, v_{iz} (i = 1,2,3), and the

normal vector n_i of the triangle mesh selected, in which n_{ii}, n_{ij}, and n_{ik} are the components of n_i along the directions of the *x*-, *y*-, and *z*-axes, respectively.

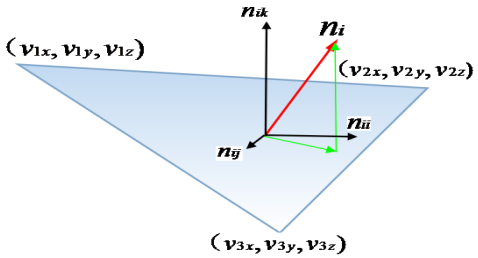

Figure 1. Triangle mesh diagram

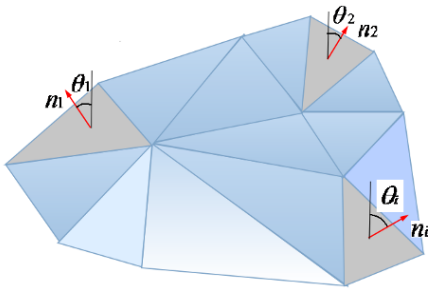

Figure 2. Selection of triangle mesh diagram of equal thickness

The vertex-redundant and edge-redundant data of triangle meshes are simplified and merged[13] on the basis of the automatically generated STL file to reduce the calculation work. The components n_{ii}, n_{ij}, and n_{ik} of the normal vector can be expressed by the vertex coordinates of the triangle meshes according to the right-hand screw rule.

$$\begin{cases} n_{ii} = (v_{1y} - v_{3y})(v_{2z} - v_{3z}) - (v_{1z} - v_{3z})(v_{2y} - v_{3y}) \\ n_{ij} = (v_{1z} - v_{3z})(v_{2x} - v_{3x}) - (v_{2z} - v_{3z})(v_{1x} - v_{3x}) \\ n_{ik} = (v_{1x} - v_{3x})(v_{2y} - v_{3y}) - (v_{2x} - v_{3x})(v_{1y} - v_{3y}) \end{cases}.$$

2.3 Rotating model and boundary constraints of the STL model

The part model can involve rotating around the *x*-, *y*-, and *z*-axes, as well as overall translation. Given that the forming angle is the angle between the normal vector and the *z*-axis and that the rotation around the *z*-axis and overall translation do not affect the size of the forming angle, only the rotation around the *x*- and *y*-axes should be considered in practical applications.

Several constraint conditions of the rotation are proposed in this work because the angle of rotation around the *x*- and *y*-axes cannot be determined in advance for a three-dimensional numerical model. First, the size of the forming angle θ at any position of the parts cannot exceed the forming limit angle $\theta_{\max}$. Second, the forming angle $\theta_i = \arccos(t_i / t_0)$ of the parts can be determined with the law of cosines for parts that require special thickness t_i. Triangle mesh is selected in this position, and the angle between the normal vector of the mesh and the *z*-axis is generated to reach θ_i after rotation. Third, triangle meshes are selected in the position that requires thickness correlation, as shown in Figure 2. For any two triangle meshes, the size of angles θ_i and θ_{i-1} can be determined with the value of the thickness difference $\Delta t = t_i - t_{i-1} = t_0(\cos\theta_i - \cos\theta_{i-1})$ when the thickness is predetermined. In particular cases, if the thicknesses of selected triangle meshes tend to be equal, that is, $\Delta t \cong 0$, then $\theta_i \cong \theta_{i-1}$.

Assuming that the autorotation angle of every step is $\Delta\theta$ in the development process, the rotation formulae around the *x*- and *y*-axes can be expressed as follows:

$$\begin{cases} y' = y\cos\Delta\theta - z\sin\Delta\theta \\ z' = y\sin\Delta\theta + z\cos\Delta\theta \\ x' = x \end{cases} \text{ and } \begin{cases} z' = z\cos\Delta\theta - x\sin\Delta\theta \\ x' = z\sin\Delta\theta + x\cos\Delta\theta \\ y' = y \end{cases}$$

The single step rotation equation of any point P around the *x*- and *y*-axes can be expressed by homogeneous coordinates as

$$\begin{bmatrix} x' \\ y' \\ z' \\ 1 \end{bmatrix} = \begin{bmatrix} 1 & 0 & 0 & 0 \\ 0 & \cos\Delta\theta & -\sin\Delta\theta & 0 \\ 0 & \sin\Delta\theta & \cos\Delta\theta & 0 \\ 0 & 0 & 0 & 1 \end{bmatrix} \cdot \begin{bmatrix} x \\ y \\ z \\ 1 \end{bmatrix} \text{ and } \begin{bmatrix} x' \\ y' \\ z' \\ 1 \end{bmatrix} = \begin{bmatrix} \cos\Delta\theta & 0 & \sin\Delta\theta & 0 \\ 0 & 1 & 0 & 0 \\ -\sin\Delta\theta & 0 & \cos\Delta\theta & 0 \\ 0 & 0 & 0 & 1 \end{bmatrix} \cdot \begin{bmatrix} x \\ y \\ z \\ 1 \end{bmatrix}$$

These coordinates are concisely expressed as $P' = R_x(\Delta\theta) \cdot P$ and $P' = R_y(\Delta\theta) \cdot P$.

In the actual rotation, the transformation position generated after two successive rotations corresponding to point P is expressed as follows:

$$P' = R(\phi_2) \cdot \{R(\phi_1) \cdot P\} = \{R(\phi_2) \cdot R(\phi_1)\} \cdot P.$$

Two successive rotations are determined to be additives by multiplying the two rotation matrices, that is, $R(\phi_2) \cdot R(\phi_1) = R(\phi_1 + \phi_2)$.

Thus, the coordinates after rotation can be calculated by using the composite transformation matrix.

$P' = R(\phi_1 + \phi_2) \cdot P.$

As such, if the component of the automatic rotation angle around the coordinate axis is set to $\Delta\theta$ every time, then the coordinate transformation formula can be easily derived after n rotations.

$P' = R(\Delta\theta_1 + \Delta\theta_2 + \cdots + \Delta\theta_n) \cdot P = R(n \cdot \Delta\theta) \cdot P.$

The initial forming angle θ of the specified position of the model is the angle between the z-axis and the normal vector of the triangle mesh selected. The process ends when the angle after rotation is obtained.

According to the component $\Delta\theta$ of the set rotation angle, the autorotation of the model can be achieved by using the inner function call of an available CAD (Computer-Aided Design)system. Taking the UG system as an example, the generation of the rotation transformation matrix requires the UF5945 rotation function of transform to be expressed as follows:

Void UF5945 (*rotate_origin*, *rotate_axis*, *rotate_angle*, *mtx*, *result*),

where rotate_angle = $\Delta\theta$, rotate_orign denotes the coordinates of the points on the rotation axis under the ABS(Absolute coordinates), rotate_axis denotes the components of the direction vector of the rotation axis under the ABS, mtx denotes the rotation matrix, and result denotes the function operation result.

3. Experimental confirmation

As shown in Figure 3, a free-curved surface part was selected for the experiment. Then, random placement was compared with optimization of the forming direction. The randomized model selected the arbitrary position as the main forming direction in the CAD system. In the optimization of the forming direction experiment, the STL mesh model of parts was obtained, as shown in Figure 4. The triangle tolerance and adjacent tolerance were both set to 0.05 mm. Four triangle meshes were symmetrically selected along the left and right sides of the model as feature points of equal thickness. The angles between the outer normal vector of the triangle mesh and the z-axis did not exceed the sheet forming limit angle θ_{max} after model rotation. In addition, the thickness of the left and right sides of parts were well-distributed.

The 1060H24 hot rolled aluminum plate was selected as the experimental material. The following parameters were set: size, 250 × 250 × 1.3 mm; measured tensile strength δ_b, 119 MPa; specified nonproportional elongation stress $\delta_{p0.2}$, 72 Mpa, elongation δ_0, more than 5%; and forming limit angle θ_{max}, 76°.

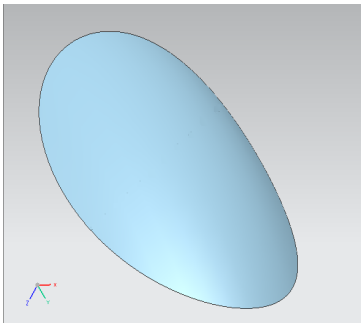

Figure 3. Model of the parts

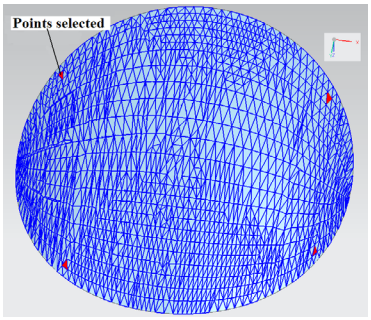

Figure 4. STL triangle mesh of the model

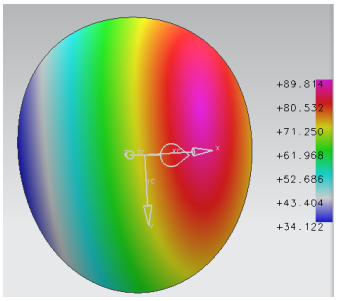

(a) random placement

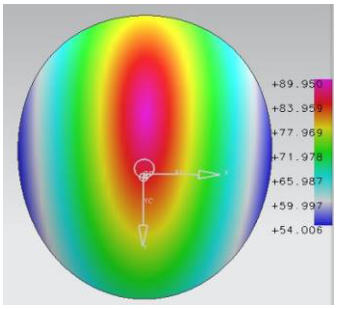

(b) optimized placement

Figure 5. Cloud charts of forming angles

The forming angle of the random placement of the forming direction is shown depicted as a cloud chart in Figure 5a. Figure 5b shows the cloud chart after an optimized rotation. The cloud chart indicates that in two positions, the forming angles of each part of the parts are within the limit of the sheet metal forming angle. In Figure 5b, the forming angles along the left and right sides of the parts are symmetric after the

optimized rotation of the forming direction.

The negative forming process method was used in the experiment. The process required the addition of the necessary addendum surface for the parts of different placements to ensure the clamping of parts and guarantee the closure of the knife track, as shown in Figures 6a and 6b.

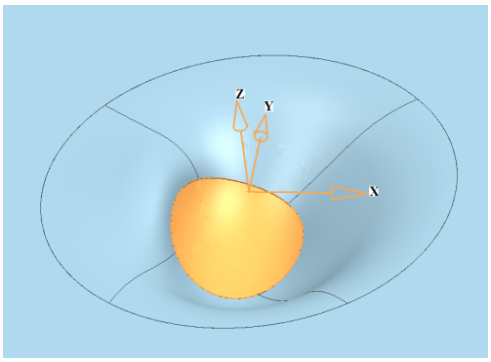

(a) position of random placement

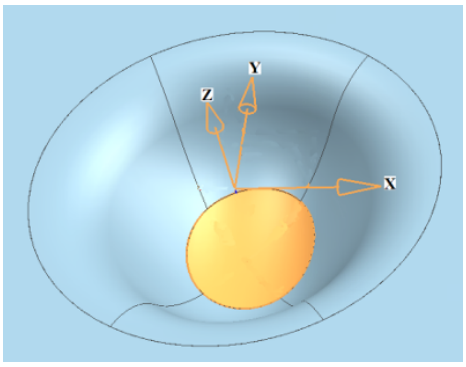

(b) position of optimized placement

Figure 6. Adding addendum surface

The parts were modeled in the UG, and the contour tool path was generated. The feed rate of each layer was 0.1 mm. In the experiment, the forming machine was an NC incremental forming machine tool proposed and developed independently by the Nanjing University of Aeronautics and Astronautics. The material of the head forming tool was high-speed steel with an end diameter of 8 mm. The experimental process is shown in Figure 7.

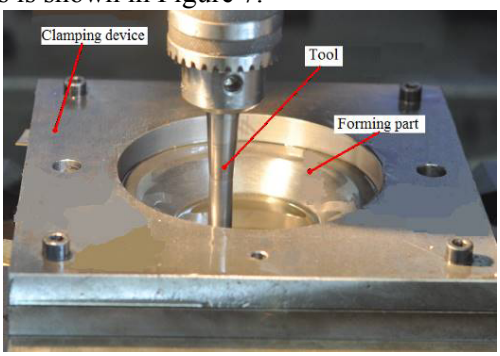

Figure 7. Processing process

The processing parts of the two types of placement are shown in Figures 8a and 8b.

(a) random placement

(b) optimized placement

Figure 8. Experimental forming

4. Experiment results

The experimental processing parts shown in Figures 8a and 8b are cut along the position shown in Figure 9. The sectional view of the parts is shown in Figure 10. A measuring instrument was used to measure the points shown in Figure 9. The measured thicknesses of the parts are shown in Tables 1 and 2.

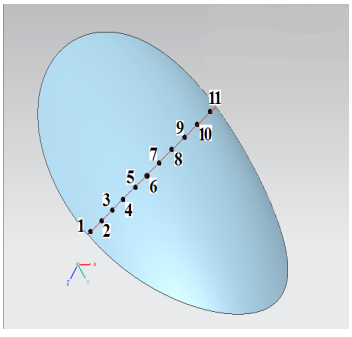

Figure 9. Thickness measuring points of the processing parts

The theoretical forming angle θ of the measuring point position was obtained on the basis of Figure 5 and then compared with the theoretical thickness. The theoretical thickness was obtained according to the

law of cosines of thickness $t = t_0 * \cos\theta$ to derive the relative error of thickness.

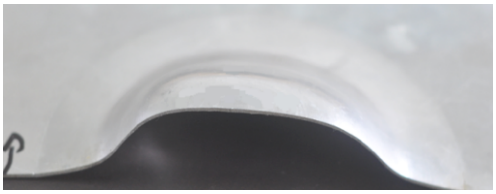

(a) random placement

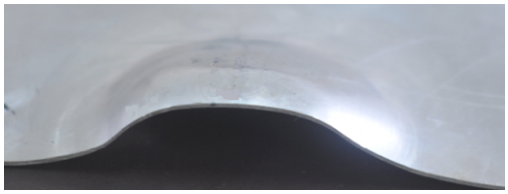

(b) optimized placement

Figure 10. Section view of the processing parts

Tables 1 and 2 and Figure 11 show that unlike in the random placement of processing parts, part thickness in the optimized placement was basically symmetric along the measuring point position. The overall thickness of the parts was also well-distributed. The thickness difference among the random placement parts was relatively large. The position achieved with the optimized placement was better than that achieved with the random placement for the stiffness and strength of forming parts. As such, the feasibility of using the STL model mesh of the parts to optimize the main forming direction was proven. In addition, on the basis of the data of the thickness errors shown in Tables 1 and 2, a certain error between the actual and theoretical thicknesses of the parts was observed. However, the overall error was small. We also verified that the thickness variation of the incremental forming parts basically follows the law of cosines $t = t_0 * \cos\theta$ but is unaffected by the forming direction of parts.

measuring point(cm)	Theoretically forming angle(°)	Theoretically thickness(mm)	Measured thickness(mm)	Thickness Error(%)
1	53.5°	0.77	0.82	6.49
2	46.2°	0.9	0.96	6.66
3	39.4°	1	1.06	6
4	33.0°	1.09	1.12	2.75
5	26.7°	1.16	1.19	2.58
6	20.5°	1.22	1.21	-0.82
7	14.3°	1.26	1.28	1.58
8	8.5°	1.28	1.2	-6.26
9	4.3°	1.29	1.27	-1.56
10	7.3°	1.29	1.21	-6.21
11	13.9°	1.26	1.19	-5.56

Table 2. The sectional thickness of parts after optimized placement

measuring point(cm)	Theoretically forming angle(°)	Theoretically thickness(mm)	Measured thickness(mm)	Thickness Error(%)
1	33.7°	1.08	1.01	-6.49
2	26.4°	1.16	1.09	-6.04
3	19.7°	1.22	1.14	-6.56
4	13.4°	1.26	1.2	-4.77
5	7.6°	1.28	1.26	-1.57
6	4.2°	1.29	1.31	1.55
7	7.6°	1.28	1.33	3.9
8	13.4°	1.26	1.23	-2.39
9	19.7°	1.22	1.18	-3.28
10	26.4°	1.16	1.12	-3.45
11	33.7°	1.08	1.06	-1.86

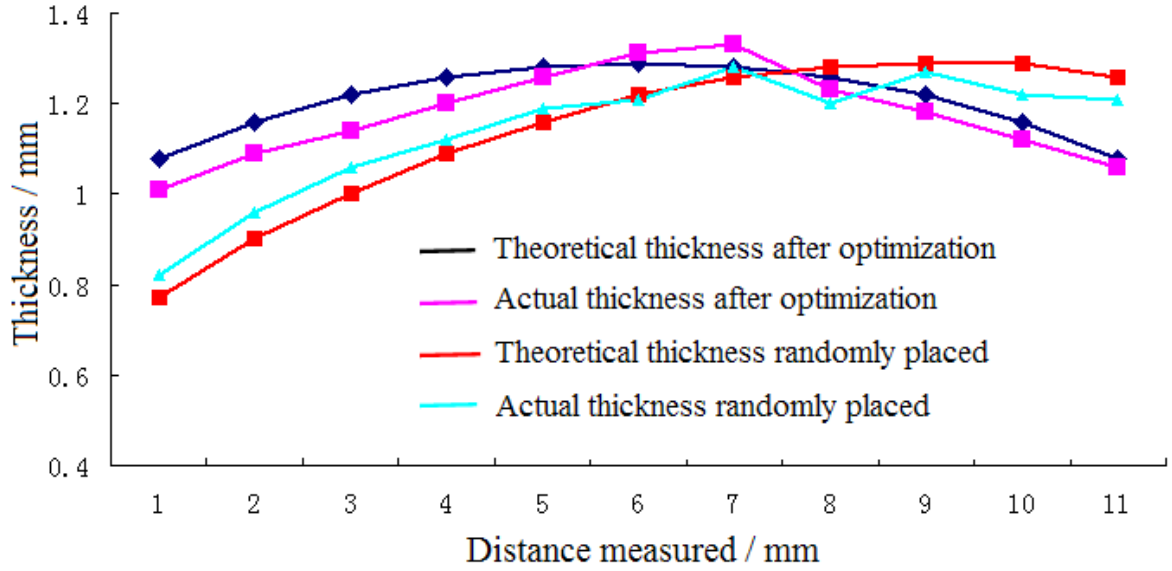

Figure 11. Distribution of part thickness

5. Conclusion

(1) The proposed method can determine the reasonable main direction of incremental forming by using the angle between the z-axis and the normal vector of the triangle mesh of the STL model as the forming angle of this position. The relationship between the normal vector of the triangle mesh and vertex is also utilized via the rotation of the specified normal vector.

(2) The experimental results show that the thickness distribution of the incremental forming parts can be effectively improved by selecting a reasonable forming direction. The experimental results also proved the feasibility of using the STL model mesh of parts to optimize the main forming direction.

(3) This study verified the relationship between the actual and theoretical thicknesses of the parts of incremental forming. The thickness variation of the incremental forming parts basically follows the law of cosines $t = t_0 * \cos\theta$, but such variation is unaffected by the placement of the position of the parts.

Acknowledgments

This work is supported by Innovation Fund Project for Nanjing University of Technology. (Project No. CKJB201304, CKJB201402, YKJ201311, and YKJ201404).

This work is supported by the Opening Project of Jiangsu Key Laboratory of Advanced Structural Materials and Application Technology. (Project No. ASMA201410 and ASMA201417).

This work is supported by Students Innovation Project of Jiangsu Province. (Project No. 201511276041Y).

References

1. Jackson KR, Allwood JM, Landert M. (2008) Incremental forming of sandwich panels. *J Mater Process Technol*, 204(1-3) , p.p.290-303.
2. Attanasio A,Ceretti E, Giardini C, et al.(2008) Asymmetric two points incremental forming: improving surface quality and geometric accuracy by tool path optimization. *Journal of Materials Processing Technology*, 197 (1- 3) , p.p.59 -67.
3. Bambach M, Taleb Araghi B, Hirt G. (2009) Strategies to improve the geometric accuracy in asymmetric single point incremental forming. *Prod Eng Res Devel*, 3(2), p.p.145-156.
4. Leszak E. Apparatus and process for incremental dieless forming [P]. US: 3342051A1, 1967.
5. Matsubara, S.A. (2001) Computer numerically controlled dieless incremental forming of a sheet metal. Proceedings of the Institution of Mechanical Engineers B. *Journal of Engineering Manufacture*, 215, p.p. 959-966.
6. S.Matsubara (1992) Nonsymmetric flaring of tube end with CNC milling machine. *JJCTP*, p.p. 581-584.
7. Micari F, Ambrogi G, Filice L. (2007) Shape and dimensional accuracy in single point incremental forming: state of the art and future trends. *J Mater Process Technol*, 191(1), p.p.390-395.
8. Hussain G, Gao L (2007) A Novel Method to Test the Thinning Limits of Sheet Metals in Negative Incremental Forming. *International Journal of Machine Tools and Manufacture*,

47(3-4) , p.p.419- 425.
9. Yamashita M, Gotoh M, Atsumi SY (2008) Numerical simulation of incremental forming of sheet metal. *Journal of Materials Processing Teghnology*, 199, p.p.163-172.
10. Jeswiet J, Micari F, Hirt G. (2005)Asymmetric single point incremental forming of sheet metal. *CIRP Annals-Manufacturing Technology*, 54(2), p.p. 88-114.
11. Hirt G, Ames J, Bambach, et al. (2004) Forming strategies and process modeling for CNC incremental sheet forming. *CIRP Annals-Manufacturing Technology*, 53(1), p.p.203-206.
12. G. Hussain, L. Gao. (2007) A novel method to test the thinning limits of sheet metals in negative incremental forming. *International Journal of Machine Tools & Manufacture*, 47, p.p.419-435.
13. Qu X Z, Brent S. (2003)A 3D surface offset method for STL-format models. *Rapid Prototyping Journal*, 9(3), p.p.133-141.

Prediction of Soil Erosion Induced Sediment Production using Fuzzy Neural Network Model

Xinyu Geng[1,2]

[1]Southwest Petroleum University, Xindu, Sichuan 610500, China
[2]State Key Laboratory of Hydraulics and Mountain River Engineering, Sichuan University, Chengdu, Sichuan 610065, China

Hualong Dai

Luzhou vocational and technical college, Luzhou, Sichuan 646005, China

Li Yang

Southwest Petroleum University, Xindu, Sichuan 610500, China